

ESTIMATING SOIL HYDRAULIC PROPERTIES USING L-BAND RADIOMETER AND GROUND-PENETRATING RADAR

Jonard F., Weihermüller L., Schwank M., Jadoon K. Z., Vereecken H., and Lambot, S.

Research Centre Jülich, Institute of Bio- and Geosciences, Agrosphere (IBG-3), Germany

ABSTRACT

In this study, we experimentally analyze the feasibility of estimating the soil hydraulic properties from L-band radiometer and ground-penetrating radar (GPR) data. L-band radiometer and ultrawideband off-ground GPR measurements were performed above a sand box in hydrostatic equilibrium with a water table located at different depths. The results of the inversions showed that the radar and radiometer signals contain sufficient information to estimate the soil water retention curve and its related hydraulic parameters with a relatively good accuracy compared to time-domain reflectometry estimates. However, an accurate estimation of the hydraulic parameters was only obtained by considering the saturated water content parameter as known during the inversion.

Index Terms— L-band radiometer, GPR, soil hydraulic parameters, soil water content, inverse modeling

1. INTRODUCTION

Soil hydraulic properties are of major interest for estimating water and energy fluxes at the land surface. In general, estimation of these properties relies on the measurement of soil water content (SWC) within the soil profile usually performed by soil sampling or with in-situ sensors such as time-domain reflectometry (TDR) or capacitance probes. However, these methods do not account for the high spatial variability, especially over large areas. On the other hand, proximal sensors such as ground-based microwave radiometer and ground-penetrating radar (GPR) can be used to obtain information at the field scale with high spatial resolution, but these measurements may be biased by confounding factors such as soil surface roughness [1, 2, 3].

The objective of this study is to experimentally analyze the feasibility of estimating the soil hydraulic properties from L-band radiometer and off-ground GPR data. In particular, we investigated the potential of radiometer and GPR to identify the hydraulic properties of a sandy soil in hydrostatic equilibrium with a water table at different depths. In this condition, the SWC profile corresponds to the soil water retention curve, which can be related to the soil hydraulic parameters

This study was supported by the German Research Foundation DFG (Transregional Collaborative Research Centre 32).

by using a simple soil hydraulic model. To the best of our knowledge, this study represents a first attempt to compare the estimation of soil hydraulic parameters from active and passive microwave remote sensing data.

2. EXPERIMENTAL SETUP

L-band radiometer and off-ground GPR measurements were performed over a 1.00-m-deep and 2.00 x 2.00 m² area wooden box filled with sand. The L-band radiometer ELBARA II was fixed on an aluminium arc at 4 m height above the ground and the antenna was pointed towards the sand box with an observation angle of 36° relative to the vertical direction (Fig. 1). The ultrawideband off-ground GPR antenna



Fig. 1. Picture of the experimental setup including a radiometer fixed on an arc and a sand box in the centre of a metal grid at the TERENO test site in Selhausen (Germany).

was fixed above the sand box on a wooden frame and the GPR antenna aperture was situated at about 0.35 to 0.40 m above the soil surface with normal incidence. GPR measurements were performed between 0.8–2.6 GHz and with a frequency step of 8 MHz. To increase the sensitivity of the radiometer to radiations emitted from the sand within the box and reduce the influence of radiance originating from areas outside, the surrounding soil surface was covered by a metal grid (area of 116 m²) with a mesh size of 0.5 cm (Fig. 1). Radiometer

and GPR measurements were performed with the water table at 7 different depths, ranging from the bottom of the box to the sand surface. For each water table depth, hydrostatic equilibrium was waited for during 6 to 11 days in order to produce a vertical water content profile above the water table in agreement with the sand water retention curve.

TDR and capacitance sensors were inserted at 7 depths, i.e., 5, 10, 20, 30, 40, 60, and 80 cm depth of two opposite sides of the box to measure the dielectric permittivity and bulk electrical conductivity within the sand box (Fig. 2).

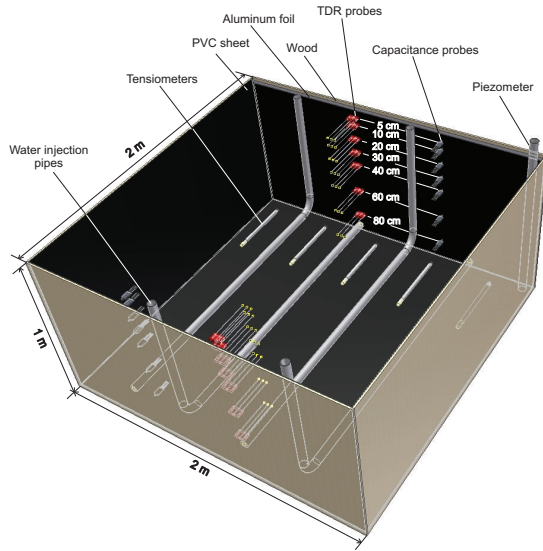


Fig. 2. Detailed sketch of the sand box.

3. MODELING APPROACH

3.1. Soil hydraulic model

In this study, radiometer and radar measurements were only performed when the sand was in hydrostatic equilibrium with a water table located at a position z_w [m]. In hydrostatic conditions, the water content profile can be described by the water retention curve of the soil, which was modeled in this study using the van Genuchten model [4] with θ_r and θ_s [$\text{m}^3 \text{m}^{-3}$] as the residual and saturated water contents, respectively, and α [m^{-1}] and n [-] as curve shape parameters.

3.2. Radiative transfer model

The brightness temperature T_B is classically expressed using a zero-order radiative approach [5]. In this study, T_B is assumed to be a linear combination of the radiance emitted from the sand box and the radiance emitted from the surrounding area:

$$T_B^p = \eta^p [(1 - R_s^p) T_s + R_s^p T_{\text{sky}}] + (1 - \eta^p) [(1 - R_0^p) T_0 + R_0^p T_{\text{sky}}] \quad (1)$$

where η is the fractional amount of the measured radiance which was emitted from the sand box, R_s [-] is the reflectivity of the sand box, R_0 [-] is the reflectivity of the surrounding area, T_{sky} [K] is the sky radiance (≈ 4.8 K), T_s [K] is the effective physical temperature of the soil in the box, T_0 [K] is the effective physical temperature of the ground surrounding the box, and p refers to the polarization (H or V). R_s represents the soil reflectivity from the sand box and can be modeled using a coherent approach considering the sand box system as a planar layered medium. The medium of the n^{th} layer is homogeneous and characterized by the dielectric permittivity ϵ_n , the electric conductivity σ_n , and the thickness h_n . The reflectivity model is based on a matrix formulation of the boundary conditions at the layer interfaces derived from Maxwell's equations [6]. To derive the reflectivity of the layer stack, the model was evaluated for dielectric layers with a thickness of 1 cm.

3.3. GPR model

The radar signal S_{11} can be expressed as the ratio between the backscattered field and incident field at the radar transmission line reference plane. The radar model used to inverse the GPR signal consists of a 3D planar layered medium (N horizontal layers) with a point source and receiver. The use of a 3D model is essential to take into account spherical divergence (geometric spreading) in wave propagation. The medium of the n^{th} layer is homogeneous and characterized by the dielectric permittivity ϵ_n , the electric conductivity σ_n , and the thickness h_n . In this study, the thickness of the layers was set to 1 cm as for the radiometer (reflectivity model). The Green's function, i.e., the solution of the 3D Maxwell equations for electromagnetic waves propagating in multilayered media, is derived by computing with a recursive scheme the TE and TM global reflection coefficients of the multilayered medium in the spectral domain. The transformation back to the spatial domain is performed by numerically evaluating a semi-infinite, complex integral [1].

3.4. Inversion procedure

Inversion of the radiometer and GPR data was performed to identify the van Genuchten soil hydraulic parameters, which define the water content profile. θ_r was fixed to 0. The water table level was also assumed to be known and used as fixed parameter during the inversions. The inverse problem was formulated in the least-squares sense and the objective function to be minimized was accordingly defined for the different sensing methods as:

$$\phi(\mathbf{b}) = (\mathbf{Y}_{\text{meas}} - \mathbf{Y}_{\text{mod}}(\mathbf{b}))^T (\mathbf{Y}_{\text{meas}} - \mathbf{Y}_{\text{mod}}(\mathbf{b})) \quad (2)$$

where \mathbf{Y}_{meas} and $\mathbf{Y}_{\text{mod}}(\mathbf{b})$ are either the measured and modeled GPR Green's functions or radiometer brightness temperature, and \mathbf{b} is the parameter vector to be estimated ($\mathbf{b} = [\theta_s, \alpha, n]$).

4. RESULTS AND DISCUSSION

4.1. Brightness temperature

Figure 3 shows the brightness temperature (T_B) measured by the L-band radiometer above the experimental setup with the free sand surface ($T_{B,sand}$), the sand surface covered by an absorber ($T_{B,abs}$), and the sand surface covered by a perfect reflector ($T_{B,refl}$). $T_{B,sand}$ decreases with increasing water table level, which results from the progressive wetting of the sand. $T_{B,refl}$ measured above the entirely grid covered setup (including the sand box covered by a copper sheet) shows similar values (15–17 K at V-pol and 12 K at H-pol) to the sky brightness temperature (≈ 4.8 K), which confirms that the metal grid used as reflector to block the emission from the surrounding area of the sand box worked properly. The remaining difference between $T_{B,refl}$ and T_{sky} may come from (1) influences from areas not covered by the metal grid, and (2) multiple reflections and emissions from the aluminium arc. $T_{B,abs}$ shows the largest brightness temperature values. The large differences between $T_{B,refl}$, $T_{B,abs}$, and $T_{B,sand}$ proves that the size of the sand box was large enough to significantly detect different L-band radiation from the sand box for different configurations (reflector, absorber, and sand) and, therefore different SWC of the sand within the box.

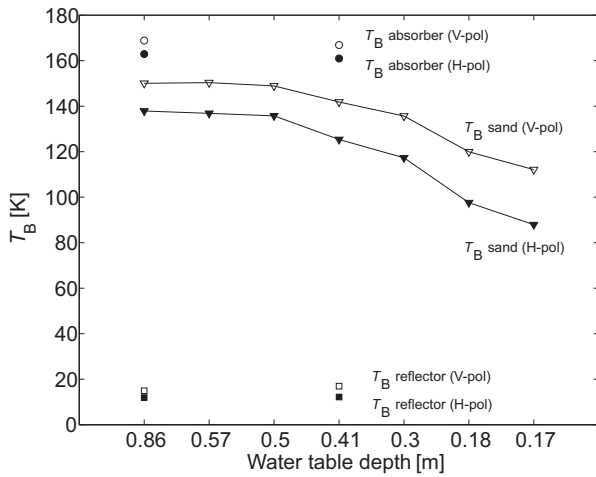


Fig. 3. T_B measured by the L-band radiometer above the free sand surface as a function of water table depth. T_B measurements above the sand surface covered by an absorber and a reflector are also shown for two calibration periods.

4.2. Radar data

Figure 4 represents the observed radar Green functions in the time domain (g_{xx}^\uparrow) for the 7 water table depths. The reflection from the soil surface is clearly visible between 2–3 ns. The surface reflection does not exactly occur at the same time

for each measurement as the height of the antenna (0.35 to 0.40 m) was slightly different for the different measurements. The amplitude of the reflection is increasing with increasing water table level, which means that the dielectric contrast between the air layer and the surface soil layer increased. No clear reflection can be observed below the surface reflection and the water table interface is also not detectable. This means that the sand dielectric profile is continuous for the frequencies used and that the electromagnetic waves are almost totally attenuated in the unsaturated zone. The assumption of a continuous dielectric profile for the unsaturated zone and an infinite lower half-space for the saturated zone in the electromagnetic model can therefore be confirmed.

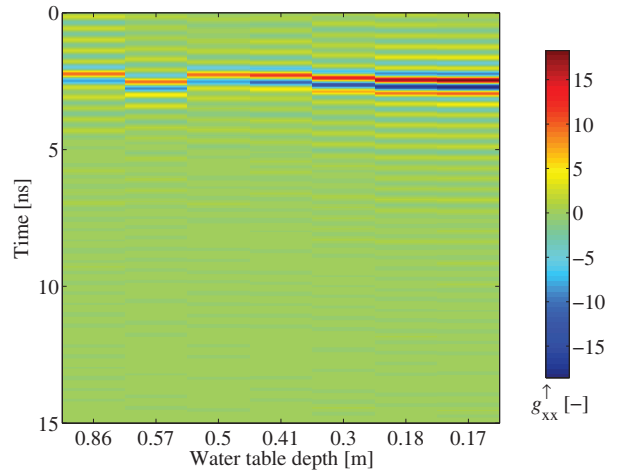


Fig. 4. Green's function in the time domain for measurements performed in the frequency range 0.8–2.6 GHz and for the seven water table depths (depth scale is not linear).

4.3. Water content profile and hydraulic parameters

The inversely estimated hydraulic parameters from the four techniques, namely, TDR, capacitance probes, radiometer, and GPR, and their corresponding confidence intervals are presented in Table 1. As TDR is widely recognized in hydrology as a reference for SWC measurement, TDR-derived parameters are considered in this study as reference parameters. The value of θ_s obtained from the inversion of the radiometer data is $0.37 \text{ m}^3 \text{ m}^{-3}$, which is slightly smaller compared to the value of $0.40 \text{ m}^3 \text{ m}^{-3}$ obtained from the inversion of the TDR data. As the confidence interval is relatively large, inversion of the hydraulic parameters was also performed by fixing θ_s to $0.40 \text{ m}^3 \text{ m}^{-3}$ in order to reduce the number of unknowns. Radiometer-derived α and n show slightly different values compared to TDR-derived parameters but the confidence intervals are relatively small (± 0.6 for α and ± 0.7 for n). The value of θ_s obtained from the inversion of GPR data is $0.27 \text{ m}^3 \text{ m}^{-3}$, which is significantly lower

Table 1. Inversely estimated van Genuchten parameters. Confidence intervals are presented in brackets ($\alpha_p = 0.05$).

	θ_s $\text{m}^3 \text{m}^{-3}$	α m^{-1}	n -
TDR	0.399 (0.011)	6.258 (0.694)	3.160 (0.456)
Capacitance sensors	0.362 (0.009)	7.025 (1.112)	2.177 (0.220)
Radiometer	0.371 (0.183)	4.778 (2.403)	3.945 (2.175)
Radiometer	0.400 (fixed)	5.106 (0.551)	3.746 (0.679)
GPR	0.272 (0.072)	5.133 (1.317)	3.714 (0.616)
GPR	0.400 (fixed)	7.142 (0.436)	3.247 (0.200)

compared to the reference value. As for the radiometer data, inversion of the hydraulic parameters from GPR data was also performed by fixing θ_s to $0.40 \text{ m}^3 \text{m}^{-3}$. GPR-derived α and n are slightly closer to TDR-derived parameters compared to radiometer-derived parameters and the confidence intervals are also smaller. This can be explained by the larger information contained in the GPR signal (1101 frequencies x 1 polarization) compared to the radiometer signal (1 frequency x 2 polarizations). However, the differences in terms of accuracy for the parameter retrieval are quite small compared to the large differences in terms of information contained in the radar and radiometer signal. In addition, θ_s was much better estimated by the radiometer compared to GPR. This probably means that more information was obtained by the radiometer compared to the radar from the soil zone close to saturation. One reason for this might be that the radar electromagnetic waves are highly attenuated and not reflected in the unsaturated zone.

Figure 5 compares the soil water retention curves retrieved by the different techniques. To compute these curves, results considering θ_s as fixed parameter for the inversion of the GPR and radiometer data were used. As shown, GPR- and radiometer-derived water retention curves are very similar to the TDR-derived water retention curve.

5. SUMMARY AND CONCLUSION

In this study, we investigated the feasibility of measuring a continuous dielectric profile in a sandy soil using off-ground GPR and L-band radiometer data. In particular, measurements were performed above a sand box in hydrostatic equilibrium with a water table located at different depths. The results of the inversions showed that the radar and radiometer signals contain sufficient information to estimate the sand water retention curve and its related hydraulic parameters with a relatively good accuracy compared to TDR estimates. However, an accurate estimation of the hydraulic parameters was only obtained by considering the saturated water content parameter as known during the inversion. Further research will focus on the inversion of GPR and radiometer data at transient conditions which are much more natural-like conditions.

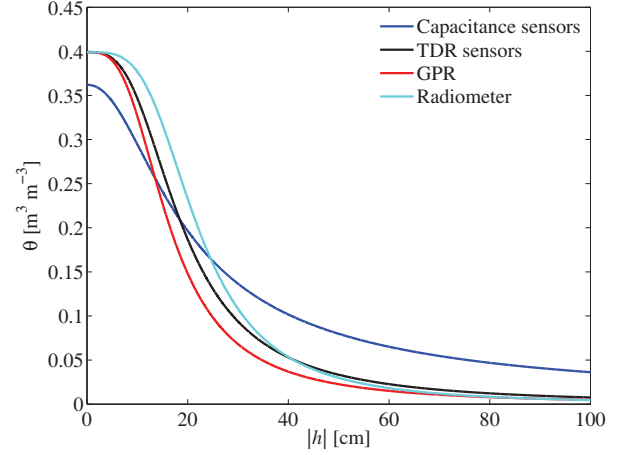


Fig. 5. Water retention curves based on the van Genuchten parametrization and estimated by the different sensing methods (capacitance sensors, TDR, GPR, and radiometer).

6. REFERENCES

- [1] S. Lambot, E. C. Slob, I. van den Bosch, B. Stockbroeckx, and M. Vanclooster, "Modeling of ground-penetrating radar for accurate characterization of subsurface electric properties," *IEEE TGRS*, vol. 42, pp. 2555–2568, 2004.
- [2] F. Jonard, L. Weihermüller, K. Z. Jadoon, M. Schwank, H. Vereecken, and S. Lambot, "Mapping field-scale soil moisture with L-band radiometer and ground-penetrating radar over bare soil," *IEEE TGRS*, vol. 49, no. 8, pp. 2863–2875, 2011.
- [3] F. Jonard, L. Weihermüller, H. Vereecken, and S. Lambot, "Accounting for soil surface roughness in the inversion of ultrawideband off-ground GPR signal for soil moisture retrieval," *Geophysics*, vol. 77, no. 1, pp. H1–H7, 2012.
- [4] M. T. van Genuchten, "A closed-form equation for predicting the hydraulic conductivity of unsaturated soils," *SSAJ*, vol. 44, pp. 892–898, 1980.
- [5] C. Mätzler, *Thermal microwave radiation: Applications for remote sensing*, IET Electromagnetic Waves series 52. The Institution of Engineering and Technology, London, 2006.
- [6] J. A. Dobrowolski, "Optical properties of films and coatings," in *Handbook of Optics*, M. Bass, E. W. Van Stryland, D. R. Williams, and W. L. Wolfe, Eds., vol. I, pp. 42.41–42.130. McGraw-Hill, New York, 1995.